FTIR microscopy reveals distinct biomolecular profile of crustacean digestive glands upon subtoxic exposure to ZnO nanoparticles

Tea Romih[1], Anita Jemec[1], Sara Novak[1], Lisa Vaccari[2], Paolo Ferraris[2,†], Martin Šimon[1,‡], Monika Kos[1], Robert Susič[3], Ksenija Kogej[3], Jernej Zupanc[1,§] Damjana Drobne*[,1]

[1]Department of Biology, Biotechnical Faculty, University of Ljubljana, Večna pot 111, 1000 Ljubljana, Slovenia

[2]Elettra-Sincrotrone Trieste S.C.p.A., S. S. 14, km 163.5 in AREA Science Park, 34149 Basovizza, Trieste, Italy

[3]Department of Chemistry and Biochemistry, Faculty of Chemistry and Chemical Technology, University of Ljubljana, Večna pot 113, 1000 Ljubljana, Slovenia

***Corresponding author:**

Damjana Drobne, University of Ljubljana, Biotechnical Faculty, Department of Biology, Večna pot 111, 1000 Ljubljana, Slovenia. Tel: + 386 1 423 33. Fax: +386 1 257 33 90. E-mail: damjana.drobne@bf.uni-lj.si

[†]*Current address:* NRE Research S.r.l., S. S. 14, km 163.5 in AREA Science Park, 34149 Basovizza, Trieste, Italy

[‡]*Current address:* College of Environment and Ecology, Xiamen University, Xiang'an Campus, Xiang'an Road (South), Xiang'an District, Xiamen, Fujian 361102, China

[§]*Current address:* SEYENS Information Solutions and Education Ltd, Krimska ulica 20, 1000 Ljubljana, Slovenia

ABSTRACT

Biomolecular profiling with Fourier-Transform InfraRed Microscopy was performed to distinguish the Zn^{2+}-mediated effects on the crustacean (*Porcellio scaber*) digestive glands from the ones elicited by the ZnO NPs. The exposure to ZnO NPs or $ZnCl_2$ (1500 and 4000 µg Zn/g of dry food) activated different types of metabolic pathways: some were found in the case of both substances, some only in the case of $ZnCl_2$, and some only upon exposure to ZnO NPs. Both the ZnO NP and the $ZnCl_2$ increased the protein (~1312 cm^{-1}; 1720-1485 cm^{-1}/3000-2830 cm^{-1}) and RNA concentration (~1115 cm^{-1}). At the highest exposure concentration of $ZnCl_2$, where the effects occurred also at the organismal level, some additional changes were found that were not detected upon the ZnO NP exposure. These included changed carbohydrate (most likely glycogen) concentrations (~1043 cm^{-1}) and the desaturation of cell membrane lipids (~3014 cm^{-1}). The activation of novel metabolic pathways, as evidenced by changed proteins' structure (at 1274 cm^{-1}), was found only in the case of ZnO NPs. This proves that Zn^{2+} is not the only inducer of the response to ZnO NPs. Low bioavailable fraction of Zn^{2+} in the digestive glands exposed to ZnO NPs further supports the role of particles in the ZnO NP-generated effects. The study provides the evidence that ZnO NPs induce their own metabolic responses in the subtoxic range.

Keywords: changed protein structure**,** *Porcellio scaber,* ZnO dissolution, square-wave voltammetry, $ZnCl_2$

INTRODUCTION

There is a general consensus in the current nanotoxicological literature that the dissolved Zn^{2+} is the main factor in the toxicity of ZnO NPs for different organisms. On the other hand, several studies could not explain all the observed effects by the dissolution of ZnO NPs, which indicates that the particles themselves may play a role (Ivask et al., 2014; Ma et al., 2013). The clear differentiation between the roles of the dissolved ions and particles in the biological effects of NPs is expected to be detected at the molecular level. At this level the interaction mode between the ions and particles is expected to be different, while the responses at the higher levels of biological complexity are common for both particles and ions. For this type of information the collective characterization and quantification of pools of biological molecules is needed.

One such method is the Fourier-Transform Infrared Microscopy (FTIRM), which provides spatially resolved information about the biochemical composition of a sample, allowing for the investigation of the functional groups that characterize a specimen. The infrared spectra of cells reflect molecular-level details regarding the concentrations, organizations, structures and (bio)chemical environments of the cellular constituents (Movasaghi et al., 2008). Analytical tools based on FTIR have been extensively employed for probing the molecular changes associated with abnormal tissues (Movasaghi et al., 2008); however, they have not been commonly implemented in the ecotoxicological studies until recently (Palaniappan and Pramod, 2010; Novak et al., 2013; Aja et al., 2014).

This study employs an experimental model, namely the digestive glands of the terrestrial isopods *Porcellio scaber,* which have previously been used to investigate the effects of nanomaterials (WO_x nanofibres) on the biomolecular profile using FTIR imaging (Novak et al., 2013). These organisms have also been used successfully to investigate the bioavailability of metals dissolved from NPs (Golobič et al., 2012; Romih et al., 2015).

The aim of the present study was to use the FTIRM on the crustacean digestive glands to investigate whether subtoxic concentrations of ZnO NPs and $ZnCl_2$ (the source of Zn^{2+}) induce distinct biomolecular profiles. We hypothesize that Zn^{2+} are not the only reason for the effects of ZnO NPs, but the effects are also governed by the ZnO particulate matter. Biomolecular profile data are accompanied by the information on the Zn bioavailability as measured by the Zn assimilation into the digestive glands.

METHODS

Preparation and characterization of the test chemicals

We used the commercially available ZnO NPs, purchased from Sigma Aldrich (St. Louis, Missouri, USA); the particles were < 100 nm in diameter with the specific surface area of 15-25 m^2/g (product no. 544906, CAS 1314-13-2). $ZnCl_2$ as a source of free Zn^{2+} was purchased from Merck (Darmstadt, Germany; product no. 1.08816.0250, CAS 7646-85-7, pro analysis grade). Stock suspensions of NPs and $ZnCl_2$ solutions at the concentrations of 1500 and 4000 μg Zn/mL were prepared in deionized water (Millipore, Billerica, Massachusetts, USA). The concentrations were chosen on the basis of our previous study (Pipan-Tkalec et al., 2010). The ZnO NPs were dispersed by a magnetic stirrer at an ambient temperature for 1 hour (400 rpm) and further sonicated in the ultrasonic bath (Sonis 2 GT ultrasound cleaner, Iskra PIO, Šentjernej na Dolenjskem, Slovenia) for 1 hour.

The characterization of the NPs was performed in ZnO nanopowder directly from the supply. Prior to the analyses, the ZnO nanopowder was attached to a holder with a double-sided adhesive carbon tape. The specimen was inspected by the field-emission scanning electron microscope ([FE-SEM] JSM-7500F, JEOL, Japan) under the accelerating voltage of 5 kV. The dispersions of ZnO NPs in milliQ (1500 and 4000 μg Zn/mL) were also inspected by the dynamic light scattering (DLS) using 3D-DLS-SLS spectrometer (LS Instruments

GmbH, Fribourg, Switzerland). Because the freshly prepared dispersions were unstable and turbid, they were allowed to settle for 1 hour prior to the measurements. The measurements were performed using 1 mL of supernatants. Details on the instrument operating parameters and data analysis are presented in the **Supplementary material** (**Method description S1**).

ZnO nanoparticle dissolution measurements

Currently, the most widely used approach for estimating the extent of dissolution of metal oxide NPs to metal ion species in aqueous suspensions comprises ultracentrifugation or filtration followed by spectroscopic determination, such as atomic absorption spectroscopy (AAS) or inductively-coupled plasma mass spectroscopy (ICP-MS) (Misra et al., 2012). The adequacy of all these methods is limited by imperfect separation by either filtering or centrifuge-assisted sedimentation, which leads to a positive error, and, on the other hand, to a loss of ions adsorbed on the filters (Xu et al., 2012). Other techniques, such as diffusion gradients in thin films and dialysis, can also give inconsistent results (Odzak et al., 2014). The free-metal-ion activity is most conveniently probed by ion-selective electrodes, but for Zn no such electrodes have been commercially available to date (Pesavento et al., 2009). In this work, we used an electrochemical method to determine the best possible approximation to free ion concentration (Jiang and Hsu-Kim, 2014). In addition to being sensitive exclusively to ion species, electrochemical methods facilitate direct determinations with minimal perturbation of the sample (Jiang and Hsu-Kim, 2014). Square-wave voltammetry (SWV) (Mirčeski et al., 2007) was used instead of the more common anodic stripping voltammetry (ASV), since the preliminary measurements featured concentrations which were well above trace level, where ASV is the method of choice.

Eight milliliters of ZnO nanopowder dispersions (1500 and 4000 μg Zn/mL) were ultracentrifuged at 100000 g for 30 minutes at 20 °C (Beckman Coulter L8-70M class H

preparative ultracentrifuge with the Type 70.1 Ti rotor and 10 mL thickwall polyallomer tubes). The supernatants were then divided into two aliquots for measuring the Zn concentrations. The first aliquot was determined by flame AAS (Perkin Elmer AAnalyst 100, Waltham, Massachusetts, USA) and the second by SWV. The Zn concentrations in the original ZnO NP dispersions were also determined by flame AAS after an overnight digestion in 1 M HNO_3 (suspension/acid ratio 1:1 v/v). All of the values were compared and the percentages of dissolved Zn^{2+} were calculated.

Square-wave voltammetry was applied using EG&G Princeton Applied Research Model 303A stationary mercury drop electrode assembly coupled with AUTOLAB PGSTAT 101 potentiostat *via* IME 303 interface. The working electrode was the hanging mercury drop electrode, the auxiliary electrode was a platinum wire, and the reference electrode was Ag/AgCl/3 mol/L KCl electrode (SSCE). In the electrolytic cell, 1 mL of 1 M, pH 7 acetate buffer was added to 4 mL of supernatant, yielding a 5 mL total volume. Before measurements, the solution was purged with N_2 for 4 minutes, and the headspace of voltammetric cell was continuously flushed with N_2 at all times to avoid O_2 interferences. The background Zn^{2+} concentration was measured before each sample by substituting supernatant with deionized water. SWV was performed without any deposition step by scanning from -0.8 V to -1.3 V *vs.* the reference electrode with 20 mV amplitude at 50 Hz and the scan rate of 100 mV/s. The scan gave rise to a peak at a median of -1.048 V *vs.* SSCE and a median full width half maximum (FWHM) of 74 mV. The method of successive standard additions was then employed, adding 100 µL of 20 µg/mL Zn^{2+} standard in each step. The Zn concentrations were finally calculated using peak heights by linear regression using the chemCal package (Ranke, 2013) for the R statistical software (R Core Team, 2013).

Test organisms

Terrestrial isopods *Porcellio scaber* (Latreille, 1804) were chosen as model organisms. Being invertebrates, they are subject to no legal restrictions. The isopods were collected in September, 2011 from a compost heap in a non-polluted garden in Podutik, Ljubljana, Slovenia. The animals were kept in a controlled chamber at a constant temperature (20 ± 2 °C) and a light regime (16 hours of light and 8 hours of darkness) and fed dry common hazel leaves (*Corylus avellana*) for three weeks before the Zn exposure. *P. scaber* adults of both sexes, including those at the intermoult and early premoult stages, were chosen for the experiments. The average fresh body weight of the animals was 44 ± 14 mg (mean ± SD; n = 100).

Experimental design

The experimental animals were divided into the following two groups: Group 1 (n = 50) was used for the analyses of Zn concentrations in digestive glands (flame AAS analyses), and Group 2 (n = 50) was processed for the FTIRM. The animals in both groups were fed Zn-spiked food for 14 days under the same experimental conditions; each group contained 10 individuals per each concentration of the tested chemical. At the end of the exposure period, Group 1 was switched to uncontaminated food for 1 day to depurate the Zn-spiked food from their digestive systems, while the animals in Group 2 were immediately dissected and processed for FTIRM.

The experimental set-up was performed as previously described (Golobič et al., 2012). During the experiment, the animals were fed dry common hazel leaves that were spiked with ZnO NPs and $ZnCl_2$. All test chemicals were freshly prepared prior to the experiment at concentrations of 1500 and 4000 μg Zn/mL. 100 μL of the test chemical per 100 mg of leaf were applied onto the abaxial leaf surfaces, which resulted in the following two final concentrations of Zn: 1500 and 4000 μg/g of dry leaf. These concentrations were chosen

based on our previous study, where they were found to be non toxic (Pipan-Tkalec et al., 2010). The leaves were left to dry at room temperature.

We inspected the ZnO NP-spiked leaves to confirm that the NPs remained on the leaves prior to the experiment. Small pieces of the ZnO-spiked leaves were attached to a holder with a double-sided adhesive carbon tape. The specimens were sputtered with gold and inspected by the thermal field-emission scanning electron microscope JSM-6500F (JEOL, Japan) under the accelerating voltage of 15 kV (**Supplementary material, Figure S1**).

Each animal was placed individually in a plastic Petri dish with 9 cm in diameter, to which individual pieces of Zn-spiked leaves were added. No substrate was used. The Petri dishes were put in a covered glass container and moisture was maintained by sprinkling the walls of the container with deionized water. The container was kept under the same controlled conditions as during the animal cultivation stage. The food was not replaced during the exposure period and fecal pellets were collected weekly. At the end of the experiments, the remnants of leaves were collected, air-dried and weighed. Fecal pellets were also weighed after drying in a desiccator for 24 hours.

After the experiment, the animals from Group 1 were dissected and the Zn concentrations in digestive glands (hepatopancreas) were measured. Each digestive gland was placed on a separate small piece of filter paper (approximately 4 mm × 7 mm in size) and was stored in a plastic tube until the analysis by flame AAS (Perkin Elmer AAnalyst 100, Waltham, Massachusetts, USA). For FTIRM only the hepatopancreas was isolated and processed for analysis.

Measurements of metal content in the food and in the animal tissues

The total Zn concentration in digestive glands of isopods from Group 1, in the uneaten leaf remnants after the experiments, and in the leaves spiked separately to serve as the

accuracy check, was determined by flame AAS. Prior to the analysis, samples were digested by a "hot plate" method in a mixture of concentrated nitric (65 % HNO_3, pro analysi, Merck, Darmstadt, Germany), and perchloric acid (70 % $HClO_4$, pro analysi, Merck, Darmstadt, Germany) (HNO_3 : $HClO_4$ = 7 : 1, vol/vol). After the evaporation of the acid, the residue was dissolved in 0.2 % HNO_3. Within each measurement a certified reference material (TORT-2, National Research Council of Canada) was used to check the accuracy and precision of the analytical procedure. Along with the samples, also 20 replicates of a known amount of a certified reference material were acid digested and each sample was measured in triplicate. The calculations followed the approach described elsewhere (Phillips et al., 2007). The Zn spiking recovery was calculated on the basis of the Zn concentration in the separately-spiked leaves and in the remnants of leaves after the experiment. All the data regarding the quality control of the experimental procedures are described and discussed in the **Supplementary material** (**Method description S2**).

Data analyses of feeding parameters and metal concentrations

Animals that died during molting and ovigerous females were excluded from further data processing (n = 7 in total). The numbers of analyzed animals are presented in the figures as part of the x-axis labels. The data are presented as the mean values, and uncertainties are expressed as standard deviations (SD). All of the data shown in the figures describe nominal concentrations of Zn (1500 and 4000 μg/g of dry leaf). The feeding rate of the isopods was calculated as the mass of consumed leaves in the 14 days of exposure divided by the mean mass of the animals used in the experiment. The statistical significances of the differences between the control and the exposed groups of animals were assessed by the Mann-Whitney *U*-test (*$p < 0.05$, **$p < 0.01$, ***$p < 0.001$), using the OriginPro 8.0 software (OriginLab Corp., Northampton, MA, USA).

220 ***FTIRM: sample preparation, data collection, pre-processing and analysis***

221 For the FTIRM, samples were prepared in the same way as in our previous study
222 (Novak et al., 2013). The digestive glands of animals from Group 2 were shock-frozen in
223 liquid nitrogen, using the Jung tissue-freezing medium (Leica Microsystems, Nussloch
224 GmbH, Nussloch, Germany). Samples were sectioned transversally into 14 µm-thick sections
225 using a Leica CM3050 cryotome (Leica Biosystems GmbH, Wetzlar, Germany), with the
226 temperature of the microtome head and chamber maintained between -25 and -20 °C. Sections
227 were placed onto 2 mm thick, IR-transparent, BaF_2 windows and transferred to the Christ
228 Alpha 2-4 LSC Freeze Dryer (Martin Christ Gefriertrocknungsanlagen GmbH, Osterode am
229 Harz, Germany) using a cryo-transfer assembly cooled with liquid N_2, and freeze-dried at -30
230 °C and 0.4 mbar for 24 hours. The samples were stored in a desiccator until the FTIRM
231 analysis was performed.

232 The FTIRM measurements were carried out at the infrared beamline SISSI
233 (Synchrotron Infrared Source for Spectroscopy and Imaging) of the Elettra-Sincrotrone
234 Trieste (Lupi et al., 2007), using the Vertex 70 interferometer coupled with the Hyperion 3000
235 Vis-IR microscope (Bruker Optics GmbH, Ettlingen, Germany). Spectra were collected from
236 cryosectioned digestive glands of animals from Group 2**.** Out of 10 exposed animals, up to 8
237 of them were selected for the FTIRM analyses. The following animals were selected: 5
238 control animals, 8 and 6 animals that were fed ZnO NPs containing 1500 and 4000 µg Zn/g of
239 dry leaf respectively, and 1 and 5 animals that were fed $ZnCl_2$ containing 1500 and 4000 µg
240 Zn/g of dry leaf respectively. One to five lyophilized cryosections per animal were measured.
241 For every cryosection, several measurement areas were chosen and divided into three regions:
242 (1) the "peripheral" region, which contained the basal membranes of the hepatopancreatic
243 cells and cytoplasmic organelles, (2) the "central" region, which included mostly the nuclear
244 and perinuclear cellular regions, and (3) the "apical" region, which contained the apical

membranes of the hepatopancreatic cells, cytoplasm and cellular cytoplasmic organelles, such as the mitochondria and ribosomes (**Supplementary material, Figure S3**). A total of 512 scans acquired in transmission mode by using the single point MCT-A detector were averaged for each measurement at a 15×15 μm lateral resolution in the wavenumber region of 4000-900 cm^{-1} to obtain one spectrum per measurement area.

Each collected spectrum was subjected to several pre-processing steps, described in detail in the **Supplementary material (Method description S3),** and only the spectra meeting the quality criteria described in Method description S3 were subjected to further analyses. The selected spectra were then analyzed using a multivariate approach with hyperSpec (Beleites, 2012), the R (R Core Team, 2013) package for handling hyperspectral data. The hierarchical cluster analysis (HCA), based on the Euclidean distances and Ward's classification algorithm, was performed on the vector-normalized absorbance spectra in the 3950-950 cm^{-1} spectral region to highlight spectral similarities and dissimilarities among the different regions of hepatopancreatic cells that were induced by the ingestion of the different Zn compounds. Cluster centroids (the average spectrum of each identified spectral family) were then compared to reveal the biochemical differences that were responsible for the classifications in addition to their second derivatives (Savitzky-Golay algorithm, 17 smoothing points), which allowed for more precise extractions of peak frequencies. The relative intensities of several diagnostic bands were compared (**Supplementary material, Table S2**), and band assignment was carried out according to the literature (Movasaghi et al., 2008).

RESULTS

Nanoparticle characteristics

Scanning electron microscopy revealed that the ZnO nanopowder was composed of particles of different sizes, ranging from tens of nanometers to several hundred nanometers (**Supplementary material, Figure S1**). The characterization of NPs in the aqueous suspension was done as suggested by the current nanoexotoxicological practice, although it is not relevant for our experimental set-up since the animals were exposed to dried NPs applied onto the leaf surface. ZnO NP size distributions were bi- or multimodal for both concentrations after one hour of settlement (**Supplementary material, Figure S2**). The average hydrodynamic diameters of the ZnO NPs in deionized water, $2\times R_h$, were separated into 60 to 80 nm and 400 to 600 nm classes. The measurements also detected objects that were larger than 1000 nm for R_h, but any size estimation in this range is unreliable; besides the number of such agglomerates was very small. The smaller sized classes were predominant in terms of mass and number (**Supplementary material, Figure S2**).

ZnO nanoparticle dissolution

ZnO NPs are among the most soluble NPs, which may significantly influence their biological effects. In this study, the measured values of dissolved Zn in aqueous ZnO NP suspensions (pH = 6.51, T = 20 °C) were lower in the case of SWV in comparison to the AAS method (**Table 1**). The ultracentrifugation under the chosen parameters was therefore not sufficient to sediment all the NPs, similarly as previously reported (Xu et al., 2013; Romih et al., 2015). The Zn concentration range that we obtained by voltammetry was similar to that reported by other researchers, namely 3.57 mg/L Zn^{2+} in 0.1 M KCl medium at pH 8 and 25 °C for uncoated ZnO NPs (David et al., 2012) or 0.3-1.3 mg/L Zn^{2+} in 81-82 mM KCl medium buffered with 20 mM 3-(*N*-morpholino)-propanesulfonic acid or piperazine-*N,N'*-bis(2-hydroxypropanesulfonic acid) at pH 8.6 and 25 °C for ZnO NPs coated with acetate, polyvinylpyrrolidone or 3-aminopropyl triethoxysilane (Jiang and Hsu-Kim, 2014). Therefore

295 we presume that the estimation of free Zn^{2+} shares by SWV was accurate. Based on the SWV,
296 the free Zn^{2+} concentrations in the ZnO NP suspensions that were used for spiking the leaves
297 for the feeding experiments represented less than 1 % of the whole Zn content (**Table 1**).
298
299 *Please insert Table 1 here.*
300
301 ***Differences among the FTIRM spectra of the digestive glands of isopods from different***
302 ***exposure groups (control, ZnO NPs or $ZnCl_2$)***
303 The HCA analysis revealed clear differences among the spectra from the controls and
304 the Zn-fed animals only at the apical regions of the cells but not in the central or peripheral
305 parts (**Supplementary material, Figure S5**), therefore only the apical regions of cells were
306 subjected to further analyses. The HCA discriminated between the controls (Cluster 1 in
307 **Figure 1A**) and the higher $ZnCl_2$ exposure concentration (Cluster 2 in **Figure 1A**), but no
308 significant differences in comparison to 1500 μg Zn/g of dry food exposure were found. In the
309 case of ZnO NP fed animals, both concentrations induced differences in FTIRM spectra
310 compared with the controls (Cluster 1 in **Figure 1B**), and result in a unique but heterogeneous
311 cluster (Cluster 2 in **Figure 1B**).
312
313 *Please insert Figure 1 here.*
314
315 In the case of ZnO NP exposure, FTIRM revealed differential spectroscopic patterns
316 mainly in the 1320–1000 cm^{-1} region, which is diagnostic for carbohydrates, nucleic acids and
317 (when the Amide III region is discernible) proteins. In the case of $ZnCl_2$ exposure, the region
318 around 3000 cm^{-1} was changed as well. The identified discriminating spectral features and
319 their biological significances are presented in **Table 2**.

320 *Please insert Table 2 here.*

321

322 **Proteins.** At higher Zn exposure (4000 µg Zn/g of dry food), both ZnO NPs and $ZnCl_2$
323 elevated the relative concentration of proteins, while protein conformational changes
324 compared to controls were found only in the case of ZnO NP exposure (**Table 2**). Proteins
325 preserve the original folding pattern, dominated by the alpha-helix motive, upon exposure of
326 animals to $ZnCl_2$ 4000 µg Zn/g of dry food, while ZnO NP exposure led to the formation of
327 more extended random protein domains (**Table 2**).

328 Several vibrational modes are diagnostic for cellular proteins (Barth, 2007). Among
329 them, Amide I and Amide II regions are considered especially relevant for describing protein
330 content and structure in complex biological systems. The Amide I (~1700-1600 cm^{-1}) region
331 represents mainly the C=O stretching of the peptide bond, with contributions from C–N
332 stretching (~10%) and N–H bending (~10%), and its position/shape is sensitive to the network
333 of hydrogen bonds involving the carbonyl group and consequently to protein secondary
334 structure. The Amide II region (~1580-1480 cm^{-1}) represents mainly the N–H bending (~60
335 %), with contributions from C–N stretching (~40 %). Even if less diagnostic than the Amide I
336 region, the Amide II region can also be deconvolved in contributions coming from helices,
337 sheets, turns and random domains that are the folding motives of cellular proteins.

338 **Protein concentration.** The area integral of the Amide I and II regions, A (1720-
339 1485cm^{-1}), is conventionally considered diagnostic for the overall protein concentration. In
340 the case of lipids, the total lipid concentration is estimated by the area integral of the
341 stretching modes of aliphatic chains, A (3000-2830cm^{-1}). The relative variations of these two
342 cellular constituents can be evaluated through the protein-to-lipid ratio A (1720-1485cm^{-1})/A
343 (3000-2830cm^{-1}), which increased upon the ingestion of both ZnO NPs and $ZnCl_2$
344 (**Supplementary material, Table S2**). This trend reveals either an increase of cellular

proteins and/or a reduction of the digestive gland lipid content. In our case, both explanations are possible, but it appears more probable that proteins increased due to an intensity increase of the Amide III band (explained in greater detail in the following paragraph).

Protein structure. With respect to the proteome profile of the apical region of the hepatopancreatic cells, no significant structural differences could be detected comparing the spectral profiles of the Amide I and II spectral bands, which peaked at the same positions for both the control animals and those that were exposed to different Zn compounds (**Figures 1D, 1F**). The Amide I band was centered at 1657 cm^{-1}, with two minor contributions at 1642 and 1688 cm^{-1}, revealing that most of the proteins in this region were helical or randomly coiled. An analogous conclusion could be drawn from the spectral invariance of the Amide II band, where the most intense contributions centered at 1545 and 1516 cm^{-1} (**Figures 1D, 1F**). However, both treated groups showed the appearance of distinctive spectral features in the 1400-1200 cm^{-1} region, which could be ascribed to specific contributions of the Amide III bands. In the Amide III region, which originates from an N–H bending and C–N stretching of the peptide backbone, different secondary structures of proteins are more resolved than in the Amides I or II (Cai and Singh, 1999). Specifically, three secondary structure frequency windows can be identified for the Amide III region (Fu et al., 1994): α-helix, 1328–1289 cm^{-1}; unordered, 1288–1256 cm^{-1}; and β-sheets, 1255–1224 cm^{-1}. However, the Amide III region is often neglected in data analysis, due to its much lower intensity when compared with Amides I and II, especially in studying complex biological systems, such as tissues or cells. Vibrational modes related to cellular carbohydrates and nucleic acids usually dominate the low wavenumber Mid IR spectral region, hiding the less intense Amide III region. However, in the investigated region of cells, the spectral contributions from nucleic acids is minor compared to other regions, which enables us to assign the contributions at 1312 cm^{-1} for all the spectral groups that underwent variation with respect to the controls upon ingestion of Zn

and at 1274 cm^{-1} for ZnO NPs at both concentrations to Amide III, related to the α-helix and the random-coiled protein domains respectively. It is to be noted that the possibility of discerning the Amide III contribution only in the treated animals supports the hypothesis of an increase in the protein concentration.

Lipids. Only in the experimental group fed $ZnCl_2$ at a higher concentration, a relative and moderate increase of the spectral intensity of the band of vinyl stretching centered at 3014 cm^{-1} could be elicited (**Table 2**). The biological significance of this change is in the desaturation of membrane lipids (**Table 2**). However, no differential spectroscopic patterns in the lipid/phospholipid relative concentration and conformational states were revealed in the animals exposed to ZnO NPs or $ZnCl_2$. Cellular lipids, and especially phospholipids, are characterized by the longest aliphatic chains and therefore their spectroscopic signatures are considered diagnostic of the cellular membranes' content, composition and order. Specifically, the shapes and positions of the methyl ($–CH_3$), methylene ($–CH_2$) and methine (–CH) C–H asymmetric and symmetric stretching bands (spectral region 3000–2830 cm^{-1}), in addition to the methyl and methylene bending modes (1480 and 1358 cm^{-1}, respectively), were unchanged upon ingestion of both ZnO NPs and $ZnCl_2$ in comparison to the control group (**Figures 1C–1F**). Moreover, both the relative intensities and positions of the carbonyl ester band of the phospholipids, centered at 1740 cm^{-1}, remained unchanged (**Figures 1D, 1F**), which is another confirmation that phospholipid concentrations and conformational states were unaffected. The ratio of the peak heights for the asymmetric stretching of methylene to that of methyl, H_{max}(2945–2894 cm^{-1})/H_{max}(2971–2950 cm^{-1}), which is diagnostic of the branching level of the aliphatic chains of lipids, did not vary significantly among the experimental groups. (**Supplementary material, Table S2**).

393 **RNA.** The major prominence of the stretching band of the C-O group of ribose,
394 centered at a discernible ~1115 cm^{-1}, common to both $ZnCl_2$ and ZnO NPs exposure, could
395 reveal an increased RNA content upon exposure to both Zn sources.
396 **Carbohydrates.** While ZnO NPs did not induce detectable effects on the cellular
397 carbohydrate pattern, $ZnCl_2$ induced an increase in the concentration of cellular sugars
398 discernable at 1043 cm^{-1} related to the C–O stretching of C–OH groups (**Table 2**). Changes in
399 this peak are commonly related to glycogen alteration (Ozek et al 2010).
400
401 **DISCUSSION**
402 The FTIRM on the crustacean digestive glands after the exposure of animals to
403 subtoxic concentrations of ZnO NPs and $ZnCl_2$ (the source of Zn^{2+}), revealed distinct
404 biomolecular profiles. In the following paragraphs, we discuss the biological significance of
405 observed changes in the biomolecular profile and conclude by linking them to the organism-
406 level responses. Data on the biomolecular profile are compared to the assimilated amount of
407 Zn in the digestive glands of *P. scaber* to elucidate the contribution of assimilated Zn ions to
408 the observed changes.
409
410 ***Biological explanation of the differences in the spectra generated by the exposure to ZnO***
411 ***nanoparticles and/or $ZnCl_2$***
412
413 **The effects generated by both ZnO NPs exposures and higher $ZnCl_2$ concentration.**
414 Altered protein-to-lipid ratios (1720-1485 cm^{-1}/3000-2830 cm^{-1}), most probably due to the
415 increase of protein content (1312 cm^{-1}) and the increased RNA content (~1115 cm^{-1}), were
416 present in both ZnO NPs exposures and the higher concentration of $ZnCl_2$. Increased protein

417 content, accompanied by the elevation of RNA, indicates an intensification of the cellular
418 metabolism.

419 Since there is no such effect present at the lower $ZnCl_2$ exposure and the concentration
420 of the dissolved Zn^{2+} in the case of ZnO was below that at the lower $ZnCl_2$ exposure, the
421 consequences of ZnO NPs exposure must have been predominantly driven by the particulate
422 matter (**Table 2**).

423

424 **ZnO nanoparticle-generated effects.** Some changes in the biomolecular profile of the
425 digestive gland cells appeared only upon ZnO NP exposure, but not in the $ZnCl_2$-fed animals.
426 Among them there are differences in the conformation of some proteins (~1274 cm^{-1}), which
427 suggests that the activation of metabolic pathways is not activated either in the controls or in
428 the $ZnCl_2$-exposed animals (**Table 2**).

429

430 **$ZnCl_2$-generated effects.** At the highest exposure concentration of $ZnCl_2$, additional
431 distinctive features in the biomolecular profile were present, which were not detected in any
432 of the ZnO NP exposures. An increased concentration of sugars (~1043 cm^{-1}), and a
433 desaturation of cell membrane lipids (at 3014 cm^{-1}) were pointed out. An increased
434 carbohydrate concentration implies alterations in carbohydrate metabolism, which is similar
435 to some other studies on mice using the metabonomic approach (Lu et al., 2011). The
436 desaturation of the cell membrane lipids indicates an altered membrane fluidity. Changes in
437 membrane fluidity are common biological responses to temperature stress, salt stress, osmotic
438 stress and/or desiccation (Los and Murata, 2004; Mahajan and Tuteja, 2005); therefore it is
439 likely that very high metal salt exposure concentrations caused a similar response (**Table 2**).

440

441 ***The link between biomolecular profile changes and organism-level responses***

With the aim to link the biomolecular profile changes with the organism-level responses, we measured feeding parameters, body mass change and mortality. A reduced feeding rate was present only at the highest exposure concentration to $ZnCl_2$ (4000 μg Zn/g of dry food) **(Figure 2**), while in none of the exposure groups animal mass or mortality were affected. The detected changes in the biomolecular profile were not propagated along the levels of biological complexity, which has already been noted in the literature (Jemec et al., 2010).

A reduction of the feeding rate at 4000 μg Zn/g of dry food in comparison to the control is in line with our previous reports, where feeding behaviour (i.e. food assimilation efficiency) was also affected in a similar experimental set-up (Pipan-Tkalec et al., 2010). This exposure concentration is therefore regarded as an adverse-effect concentration. However, at this exposure, no evidence of lipid peroxidation could be discerned from the biomolecular profile, particularly from the ratios of carbonyl stretching to methyl and methylene deformations (1740/1456 cm^{-1}) (LeVine and Wetzel, 1998, Vileno et al., 2010). Also, no occurrence of oxidative processes was revealed from the absence of downshifts of the carbonyl band at ~1740 cm^{-1} or the decreases in the methyl- and methylene-to-carbonyl ratios (1456/1400 cm^{-1}) (Di Giambattista et al., 2011). Our results show that lipid peroxidation does not necessarily accompany adverse effects at the organism level, although lipid peroxidation is commonly interpreted as an indication of adverse effects at the bimolecular level (Lushchak, 2011).

Please insert Figure 2 here

Bioaccumulation studies were performed in order to assess the bioavailable fraction of Zn for isopods. In the animals that were fed $ZnCl_2$, the Zn concentration in hepatopancreas

467 increased statistically significantly at both exposure concentrations. However, in animals fed
468 ZnO NPs, no Zn assimilation was detected. This is in accordance with the dissolution
469 assessment, where the dissolved fraction of ZnO NPs in the aqueous suspension was less than
470 1 % (at 1500 and 4000 μg Zn/g of dry food), and supports the finding that Zn^{2+} are not the
471 sole source of biomolecular profile changes after the exposure to ZnO NPs.
472
473 *Please insert Figure 3 here*
474
475 **CONCLUSIONS**
476 Our results show that ZnO particulate matter induces biomolecular profile changes in the
477 digestive glands of *P. scaber* and that Zn^{2+} is not the only reason for the effects of ZnO NPs.
478 This was confirmed by the substantially altered biomolecular profile which was accompanied
479 by a very low assimilated fraction of Zn in the animals exposed to ZnO NPs. The subtoxic
480 ZnO NPs exposure induces digestive gland biomolecular profile changes that are in part
481 particulate-matter specific (distinct protein conformation) and in part a non-specific response
482 to the external stimulus, which is present in both ZnO NPs and $ZnCl_2$ exposures (increased
483 protein and RNA content).
484

ACKNOWLEDGMENTS

The paper is part of the PhD work of Tea Romih, who received funding from Ministry of Education, Science and Sport of the Republic of Slovenia by the grant "Innovative scheme of co-funding doctoral studies for promoting co-operation with the economy and solving contemporary social challenges" under Grant Number 1291. The research was also funded by the Slovenian Research Agency (ARRS; J1-4109) and the EU FP7 nanoMILE project (Grant agreement: 310451; Call ID: FP7-PEOPLE-2013-ITN). The authors would like to thank Professor Marjan Veber from the Faculty of Chemistry and Chemical Technology for providing us with an access to his lab; Vesna Arrigler, Zdenka Držaj, Jolanda Furlan and Mojca Žitko from the same faculty for their technical assistance; and Matej Hočevar from the Institute of Metals and Technologies for the access to the electron microscopy.

DECLARATION OF INTEREST STATEMENT

The authors report no conflict of interest. The authors alone were responsible for the content and the writing of the paper.

REFERENCES

Aja M, Jaya M, Vijayakumaran Nair K, Joe IH. 2014. FT-IR spectroscopy as a sentinel technology in earthworm toxicology. Spectrochim Acta A 120:534–541.

Barth A. 2007. Infrared spectroscopy of proteins. Biochim Biophys Acta 1767:1073–1101.

Beleites C, (2012). hyperSpec: A package to handle hyperspectral data sets in R, R package v. 0.98-20120725. Department of Spectroscopy and Imaging, Institute of Photonic Technologies, Jena, Germany. Available at: http://hyperspec.r-forge.r-project.org/index.html

Cai S, Singh BR. 1999. Identification of b-turn and random coil amide III infrared bands for secondary structure estimation of proteins. Biophys Chem 80:7–20.

Cai S, Singh BR. 2004. A distinct utility of the amide III infrared band for secondary structure estimation of aqueous protein solutions using partial least squares methods. Biochemistry 43:2541–2549.

David CA, Galceran J, Rey-Castro C, Puy J, Companys E, Salvador J, Monné J, Wallace R, Vakourov A. 2012. Dissolution kinetics and solubility of ZnO nanoparticles followed by AGNES. J Phys Chem C 116:11758–11767.

Di Giambattista L, Pozzi D, Grimaldi P, Gaudenzi S, Morrone S, Castellano AC. 2011. New marker of tumor cell death revealed by ATR-FTIR spectroscopy. Anal Bioanal Chem 399:2771−2778.

Fabian H, Jackson M, Murphy L, Watson PH, Fichtner I, Mantsch HH. 1995. A comparative infrared spectroscopic study of human breast tumors and breast tumor cell xenografts. Biospectroscopy 1:37–45.

Fu F-N, DeOliveira DB, Trumble WR, Sarkar HK, Singh BR. 1994. Secondary structure estimation of proteins using the amide III region of Fourier transform infrared

525 spectroscopy: Application to analyze calcium-binding-induced structural changes in
526 calsequestrin. Appl Spectrosc 48:1432–1441.
527 Golobič M, Jemec A, Drobne D, Romih T, Kasemets K, Kahru A. 2012. Upon exposure to Cu
528 nanoparticles, accumulation of copper in the isopod *Porcellio scaber* is due to the
529 dissolved Cu ions inside the digestive tract. Environ Sci Technol 46:12112−12119.
530 Huleihel M, Salman A, Erukhimovitch V, Jagannathan R, Hammody Z, Mordechai S. 2001.
531 Novel optical method for study of viral carcinogenesis in vitro. J Biochem Biophys
532 Methods 50:111–121.
533 Ivask A, Juganson K, Bondarenko O, Mortimer M, Aruoja V, Kasemets K, Blinova I,
534 Heinlaan M, Slaveykova V, Kahru A. 2014. Mechanisms of toxic action of Ag, ZnO
535 and CuO nanoparticles to selected ecotoxicological test organisms and mammalian cells
536 in vitro: A comparative review. Nanotoxicology 8:57–71.
537 Jemec A, Drobne D, Tišler T, Sepčić K. 2010. Biochemical biomarkers in environmental
538 studies-lessons learnt from enzymes catalase, glutathione S-transferase and
539 cholinesterase in two crustacean species. Environ Sci Pollut Res Int 17:571–581.
540 Jiang C, Hsu-Kim H. 2014. Direct *in situ* measurement of dissolved zinc in the presence of
541 zinc oxide nanoparticles using anodic stripping voltammetry. Environ Sci: Processes
542 Impacts 16:2536−2544.
543 LeVine SM, Wetzel DL. 1998. Chemical analysis of multiple sclerosis lesions by FT-IR
544 microspectroscopy. Free Radical Bio Med 25:33−41.
545 Liljeblad JF, Bulone V, Tyrode E, Rutland MW, Johnson CM. 2010. Phospholipid
546 monolayers probed by vibrational sum frequency spectroscopy: instability of
547 unsaturated phospholipids. Biophys J 98:L50–L52.
548 Los DA, Murata N. 2004. Membrane fluidity and its roles in the perception of environmental
549 signals. Biochim Biophys Acta 1666:142–157.

550 Lu X, Tian Y, Zhao Q, Jin T, Xiao S, Fan X. 2011. Integrated metabonomics analysis of the
551 size-response relationship of silica nanoparticles-induced toxicity in mice.
552 Nanotechnology 22:055101 (16pp).
553 Lupi S, Nucara A, Perucchi A, Calvani P, Ortolani M, Quaroni L, Kiskinova M. 2007.
554 Performance of SISSI, the infrared beamline of the ELETTRA storage ring. J Opt Soc
555 Am B 24:959–964.
556 Lushchak VI. 2011. Environmentally induced oxidative stress in aquatic animals. Aquat
557 Toxicol 101:13–30.
558 Ma H, Williams PL, Diamond SA. 2013. Ecotoxicity of manufactured ZnO nanoparticles − A
559 review. Environ Pollut 172:76–85.
560 Mahajan S, Tuteja N. 2005. Cold, salinity and drought stresses: An overview. Arch Biochem
561 Biophys 444:139–158.
562 Mirčeski V, Komorsky-Lovrić Š, Lovrić M. (2007). Square-wave voltammetry – Theory and
563 application. Berlin Heidelberg, Germany: Springer-Verlag.
564 Misra SK, Dybowska A, Berhanu D, Luoma SN, Valsami-Jones E. 2012. The complexity of
565 nanoparticle dissolution and its importance in nanotoxicological studies. Sci Total
566 Environ 438:225–232.
567 Movasaghi Z, Rehman S, ur Rehman I. 2008. Fourier transform infrared (FTIR) spectroscopy
568 of biological tissues. Appl Spectrosc Rev 43:134−179.
569 Novak S, Drobne D, Vaccari L, Kiskinova M, Ferraris P, Birarda G, Remškar M, Hočevar M.
570 2013. Effect of ingested tungsten oxide (WO_X) nanofibers on digestive gland tissue of
571 *Porcellio scaber* (Isopoda, Crustacea): Fourier transform infrared (FTIR) imaging.
572 Environ Sci Technol 47:11284−11292.
573 Odzak N, Kistler D, Behra R, Sigg L. 2014. Dissolution of metal and metal oxide
574 nanoparticles in aqueous media. Environ Pollut 191:132–138.

575 Ozek NS, Tuna S, Erson-Bensana AE, Severcan F. 2010. Characterization of microRNA-
576 125b expression in MCF7 breast cancer cells by ATR-FTIR spectroscopy. Analyst
577 135:3094−3102.
578 Palaniappan PR, Pramod KS. 2010. FTIR study of the effect of $nTiO_2$ on the biochemical
579 constituents of gill tissues of zebrafish (*Danio rerio*). Food Chem Toxicol
580 48:2337−2343.
581 Pesavento M, Alberti G, Biesuz R. 2009. Analytical methods for determination of free metal
582 ion concentration, labile species fraction and metal complexation capacity of
583 environmenal waters: A review. Anal Chim Acta 631:129–141.
584 Phillips KM, Wolf WR, Patterson KY, Sharpless KE, Holden JM. 2007. Reference materials
585 to evaluate measurement systems for the nutrient composition of foods: results from
586 USDA's National Food and Nutrient Analysis Program (NFNAP). Anal Bioanal Chem
587 389:219–229.
588 Pipan-Tkalec Ž, Drobne D, Jemec A, Romih T, Zidar P, Bele M. 2010. Zinc bioaccumulation
589 in a terrestrial invertebrate fed a diet treated with particulate ZnO or $ZnCl_2$ solution.
590 Toxicology 269:198−203.
591 R Core Team, (2013). R: A language and environment for statistical computing. R Foundation
592 for Statistical Computing, Vienna, Austria. Available at: http://www.r-project.org/
593 Ranke J, (2013). chemCal: Calibration functions for analytical chemistry, R package version
594 0.1-29. University of Bremen, Bremen, Germany. Available at: http://cran.r-
595 project.org/web/packages/chemCal/index.html
596 Romih T, Drašler B, Jemec A, Drobne D, Novak S, Golobič M, Makovec D, Susič R, Kogej
597 K. 2015. Bioavailability of cobalt and iron from citric-acid-adsorbed $CoFe_2O_4$
598 nanoparticles in the terrestrial isopod *Porcellio scaber*. Sci Total Environ 508:76−84.

599 Vileno B, Jeney S, Sienkiewicz A, Marcoux PR, Miller LM, Forro L. 2010. Evidence of lipid
600 peroxidation and protein phosphorylation in cells upon oxidative stress photo-generated
601 by fullerols. Biophys Chem 152:164−169.
602 Whelan DR, Bambery KR, Heraud P, Tobin MJ, Diem M, McNaughton D, Wood BR. 2011.
603 Monitoring the reversible B to A-like transition of DNA in eukaryotic cells using
604 Fourier transform infrared spectroscopy. Nucleic Acids Res 39:5439–5448.
605 Xu M, Li J, Hanagata N, Su H, Chen H, Fujita D. 2013. Challenge to assess the toxic
606 contribution of metal cation released from nanomaterials for nanotoxicology–the case of
607 ZnO nanoparticles. Nanoscale 5:4763–4769.
608 Yang Y, Sulé-Suso J, Sockalingum GD, Kegelaer G, Manfait M, El Haj AJ. 2005. Study of
609 tumor cell invasion by Fourier transform infrared microspectroscopy. Biopolymers
610 78:311–317.
611
612
613

TABLES WITH CAPTIONS

Table 1. The amount of total Zn content in the suspensions used for the feeding experiments, and concentrations of Zn^{2+} as assessed by ultracentrifugation combined with either flame atomic absorption spectroscopy (AAS) or square-wave voltammetry (SWV).

Test chemical	**Nominal Zn concentration (mg/L)**	**Total Zn concentration, measured by AAS (mg/L), average ± SD, n = 4**	**Zn^{2+} concentration in the supernatant, measured by AAS (mg/L), average ± SD, n = 5**	**Zn^{2+} concentration in the supernatant, measured by SWV (mg/L), average ± SD, n = 5**	**Dissolved Zn fraction according to SWV (%)**
nano ZnO	1500	1630 ± 200	5.7 ± 0.4	3.43 ± 0.06	0.21
	4000	3080 ± 210	8 ± 1	3.9 ± 0.3	0.13
$ZnCl_2$	1500	1430 ± 50	1350 ± 80	Not measured	NA
	4000	3750 ± 90	3820 ± 50	Not measured	NA

NA – not available

623 **Table 2.** The FTIRM spectroscopic features of the *P. scaber* digestive glands that differed among the animals exposed to ZnO NPs and those exposed to $ZnCl_2$ in comparison

624 to the control. Abbreviations: A, area integral; ν, stretching.

625

Features of the FTIRM spectra	**Spectroscopic annotation**	**Biological significance**	**Changes in positions, shapes and/or relative intensity in comparison to the control**			
			ZnO NPs 1500 µg Zn/g of dry food	**$ZnCl_2$ 1500 µg Zn/g of dry food**	**ZnO NPs 4000 µg Zn/g of dry food**	**$ZnCl_2$ 4000 µg Zn/g of dry food**
1274 cm^{-1}	Amide III contribution	Conformation of proteins: mostly random domains[a,b]	Band appears	None	Band appears	None
A(1720-1485cm^{-1}) /A(3000-2830cm^{-1})	Protein-to-lipid ratio	Changed relative amount of proteins to lipids	Ratio increased	None	Ratio increased	Ratio increased
1312 cm^{-1}	Amide III contribution	Conformation of proteins: mostly alpha-helix folding patterns[a,c]	The band is more clearly distinguishable	None	The band is more clearly distinguishable	The band is more clearly distinguishable
~1115 cm^{-1}	ν (C–O) of C–OH groups of ribose[d]	Variations in RNA cellular content[e]	Band more prominent	None	Band more prominent	Band more prominent
3014 cm^{-1}	ν (=CH)	Desaturation of cell membrane	None	None	None	Increased

		lipids[f]; membrane fluidity[g]				relative band intensity
1043 cm^{-1}	C–O stretching of C–OH groups of glycogen, and carbohydrates in general[h]	Changed carbohydrates concentration	None	None	None	Increased relative band intensity

626 [a]Fu et al., 1994; [b]Cai and Singh, 2004; [c]Cai and Singh, 1999; [d]Fabian et al., 1995; [e]Whelan et al., 2011; [f]Liljeblad et al., 2010; [g]Los and Murata, 2004; [h]Huleihel et al., 2001

627 **FIGURES**

628

629 **Figure 1**

630

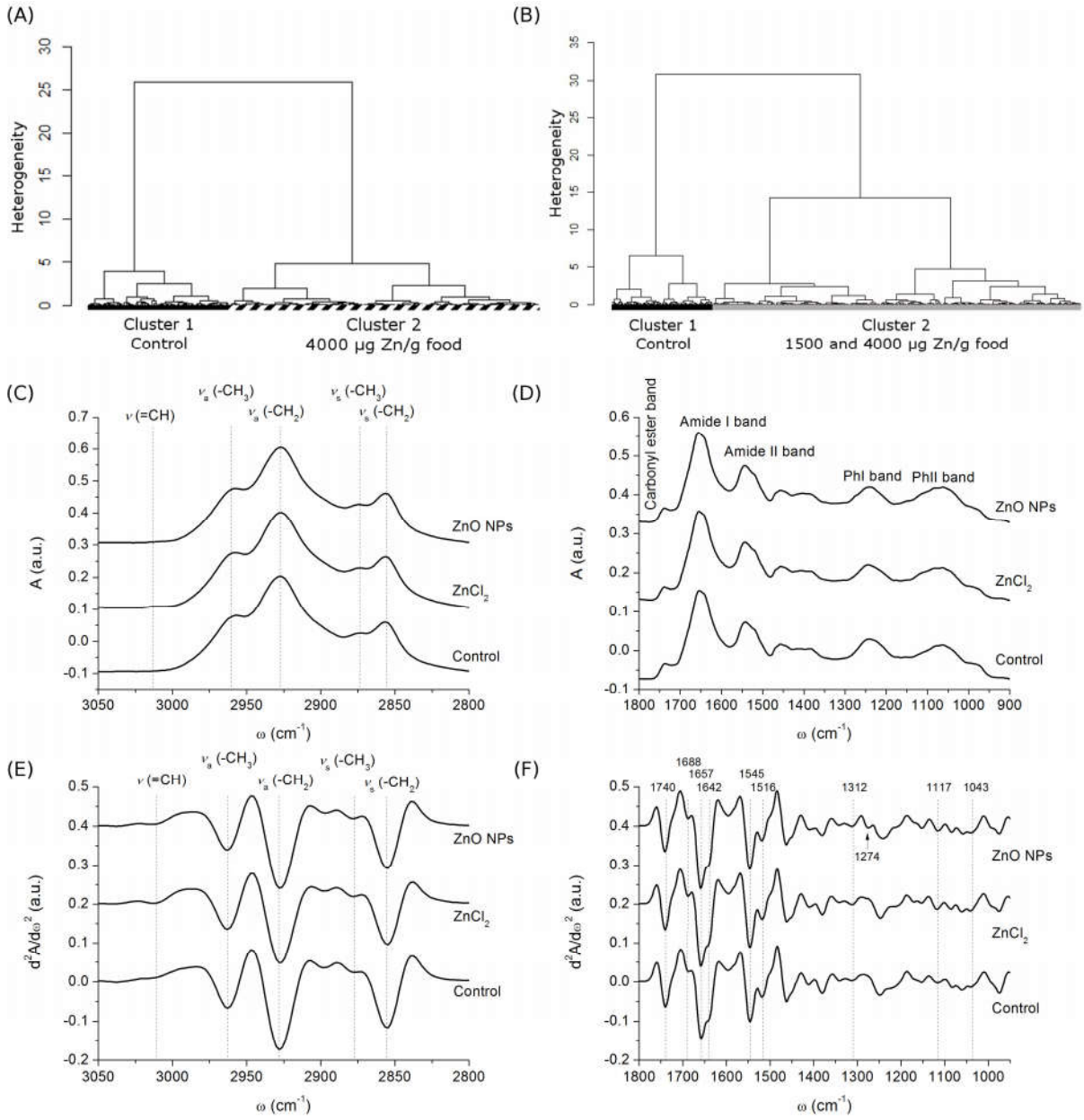

631

632

633 **Figure 2**

634

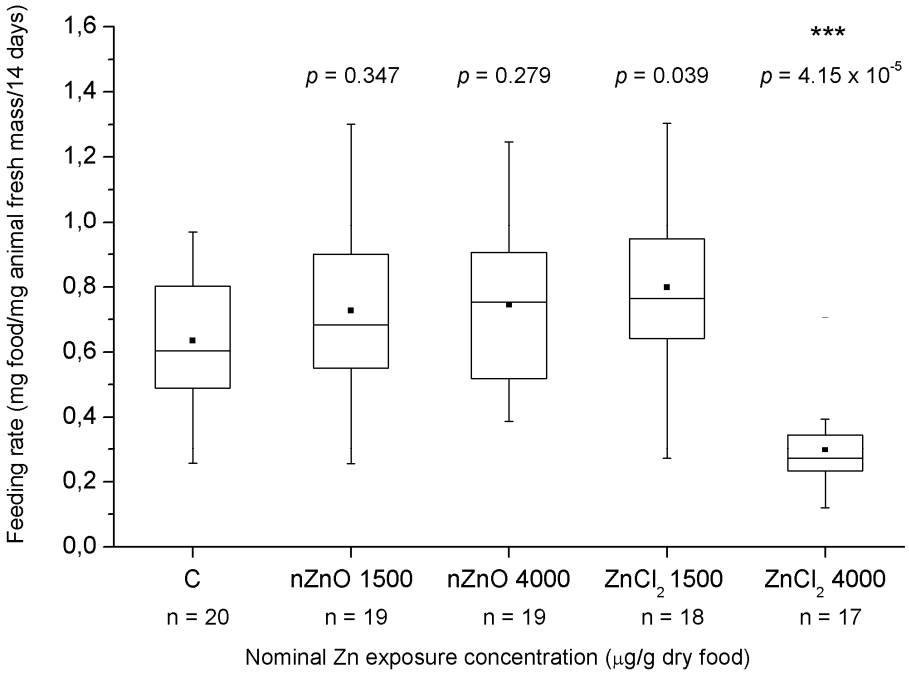

635

636

637 **Figure 3**

638

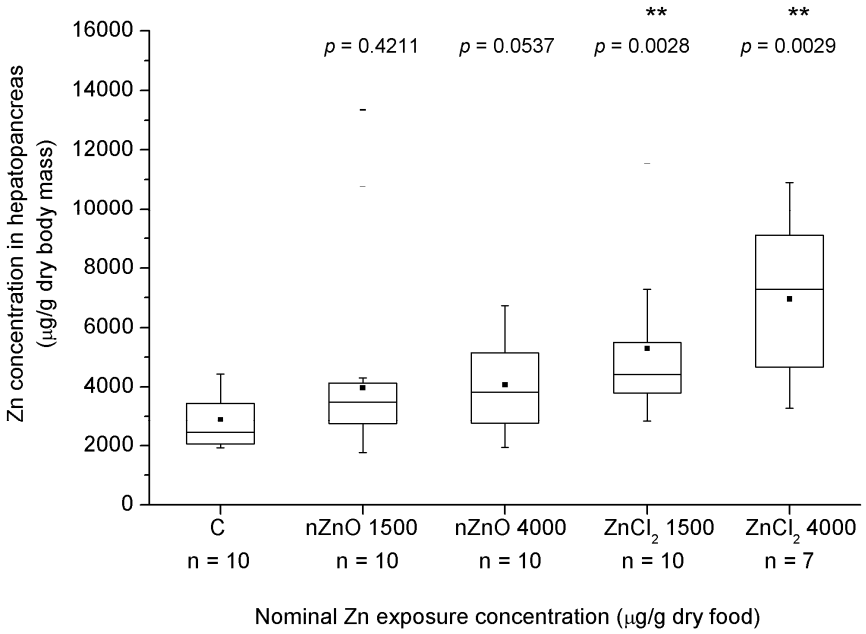

639

640

641 **FIGURE CAPTIONS**

642

643 **Figure 1.** Results of the FTIRM data analysis. **(A)** Dendrogram of the spectral heterogeneity
644 of the apically sampled points of the control animals (cluster 1, black bar) and the animals that
645 were fed $ZnCl_2$ in 4000 µg Zn/g of dry food (cluster 2, dashed bar) as revealed by the HCA
646 using vector-normalized absorbance spectra in the 3950-950 cm^{-1} region. The data for $ZnCl_2$
647 in 1500 µg Zn/g of dry food are not shown since no significant differences were found in
648 comparison to the controls. **(B)** Dendrogram of the spectral heterogeneity of the apically
649 sampled points of the control animals (cluster 1, black bar) and the animals that were fed ZnO
650 NPs in 1500 and 4000 µg Zn/g of dry food (cluster 2, gray bar) as revealed by the HCA using
651 vector-normalized absorbance spectra in the 3950-950 cm^{-1} region. **(C)-(D)** Cluster centroids
652 belonging to the apical regions of the controls (label: Control) and to the apical regions of the
653 Zn-exposed samples, $ZnCl_2$ in 4000 µg Zn/g of dry food (label: $ZnCl_2$) and ZnO NPs in 1500
654 and 4000 µg Zn/g of dry food combined (label: ZnO NPs) for the spectral regions of 3050-
655 2800 **(C)** and 1800-900 cm^{-1} **(D)**. **(E)-(F)** The second derivative of cluster centroids (17
656 smoothing points, Savitzky-Golay algorithm) for the spectral regions of 3050-2800 **(E)** and
657 1800-900 cm^{-1} **(F)**.

658

659 **Figure 2.** Feeding rates (mg food/mg animal fresh mass/14 days) of *P. scaber* isopods after
660 feeding for 14 days on Zn-spiked food. The animals were fed non-spiked food (control, C) or
661 food that was spiked with ZnO nanoparticles (1500 nZnO and 4000 nZnO, per nominal Zn
662 concentrations) or $ZnCl_2$ salts (1500 $ZnCl_2$ and 4000 $ZnCl_2$, per nominal Zn concentrations).
663 The treatments previously divided into Group 1 (for the AAS) and Group 2 (for the FTIRM),
664 are combined. The nominal exposure concentrations of Zn are provided on the x-axis. The
665 symbols on the box plot represent maximum and minimum values (whiskers: ⊥), mean values
666 (■), outliers (—), $p < 0.05$ (*) and $p < 0.001$ (***); n= number of specimens in each test group.

667

668 **Figure 3.** Concentrations of Zn in hepatopancreases of *P. scaber* isopods after feeding for 14
669 days on Zn-spiked food (**Group 1**). The animals were fed non-spiked food (control, C) or
670 food that was spiked with ZnO nanoparticles (1500 nZnO and 4000 nZnO) or $ZnCl_2$ salts
671 (1500 $ZnCl_2$ and 4000 $ZnCl_2$). The nominal exposure concentrations of Zn are provided on
672 the x-axis. The symbols on the box plot represent maximum and minimum values
673 (whiskers:⊥), mean values (■), outliers (—), and $p < 0.01$ (**); n= number of specimens in
674 each test group.

SUPPLEMENTARY MATERIAL

The Supplementary material features the detailed descriptions of methods and results not described in the manuscript, including TEM micrographs of ZnO NPs from the supply and after application on the leaves; dynamic light scattering measurements of the supernatants from the dispersions of ZnO NPs; quality control of the experimental procedures (accuracy and precision of the AAS measurements and metal spiking recovery); and details of the FTIRM data preprocessing and analysis.